

Accepted Article

Title: A High Performing Zn-ion Battery Cathode Enabled by in-situ Transformation of V2O5 Atomic Layers

Authors: Kevin Huang, Yanying Lu, Tainyu Zhu, Wessel van den Bergh, and Morgan Stefik

This manuscript has been accepted after peer review and appears as an Accepted Article online prior to editing, proofing, and formal publication of the final Version of Record (VoR). This work is currently citable by using the Digital Object Identifier (DOI) given below. The VoR will be published online in Early View as soon as possible and may be different to this Accepted Article as a result of editing. Readers should obtain the VoR from the journal website shown below when it is published to ensure accuracy of information. The authors are responsible for the content of this Accepted Article.

To be cited as: Angew. Chem. Int. Ed. 10.1002/anie.202006171

Link to VoR: https://doi.org/10.1002/anie.202006171

A High Performing Zn-ion Battery Cathode Enabled by *in-situ* Transformation of V₂O₅ Atomic Layers

Yanying Lu,[a] Tainyu Zhu,[b] Wessel van den Bergh,[b] Morgan Stefik,[b] Kevin Huang,[a]*

[a] Dr. Y. Lu, Prof. K. Huang, Department of Mechanical Engineering University of South Carolina, Columbia, SC E-mail: Huang46@cec.sc.edu [b] Dr. Zhu, Dr. W.Bergh, Dr. M. Stefik, Department of Chemistry and Biochemistry University of South Carolina, Columbia, SC

Abstract: Developing high capacity and stable cathodes is a key to successful commercialization of aqueous Zn-ion batteries (ZIBs). Pure layered V₂O₅ has a high theoretical capacity (585 mAh/q), but it suffers severe capacity decay. Pre-inserting cations into V₂O₅ can substantially stabilize the performance, but at an expense of lowered capacity. Here we show that an atomic layer deposition derived V₂O₅ can be an excellent ZIB cathode with high capacity and exceptional cycle stability at once. We report for the first time a rapid in-situ onsite transformation of V_2O_5 atomic layers into $Zn_3V_2O_7(OH)_2\cdot 2H_2O$ (ZVO) nanoflake clusters, also a known Zn-ion and proton intercalatable The extraordinary material. electrochemical performance arises from the unique attributes of the ALD-V₂O₅: high concentration of reactive sites, strong bonding to the conductive substrate, nanosized thickness and binder-free composition, all of which facilitate ionic transport and promote the best utilization of the active material. We also provide new insights into the V2O5dissolution mechanisms for different Zn-salt aqueous electrolytes and their implications to the cycle stability. Our work offers an appealing engineering solution to develop high-capacity and stable cathodes for commercial ZIBs and contributes to the fundamental understanding of ionic storage mechanisms in rechargeable aqueous batteries.

Introduction

With the fast-growing renewable industry and strong demand for leveling variable renewable power generation, rechargeable battery systems with high capacity, long cycle life, low cost, safety and eco-friendliness are highly desirable. [1] Rechargeable Zn-ion batteries (ZIBs) with mildly-acidic-to-neutral Zn-salt aqueous electrolytes, layer-structured oxide cathodes and Zn-metal anodes are some of the best contenders to meet the above requirements because of their inherent advantages in electrolyte conductivity, manufacturability, safety, cost and dendrite resistance. [2]

The current ZIBs research is mostly focused on developing high-capacity and durable cathodes. [3] While new cathode materials are currently being identified, e.g. NASICON-structured oxide, [3c] the two most studied families of ZIB cathodes are MnO₂ and V₂O₅ based materials that possess tunnel/layered structures containing abundant low-energy crystallographic sites suitable for storing Zn²⁺ and/or H⁺. [4] However, the discharge profiles for the two systems are discernably different, viz. MnO₂-based cathodes typically exhibit high and flat potentials, whereas V₂O₅-based cathodes display low and sloping potentials. [4a, 5] The difference is fundamentally rooted in their intercalation chemistries, *i.e.* redox potentials

(Mn⁴⁺/Mn³⁺ vs V⁵⁺/V⁴⁺/V³⁺) and phase composition (conversion-based multi-phase vs intercalation-based single-phase). [6] In particular, pure V_2O_5 is attractive benefitted from its highest theoretical capacity capacity (589 mAh g⁻¹ based on V⁵⁺/V³⁺ redox couple) in all V-based cathodes. However, V_2O_5 suffers cycle stability issues, largely due to its dissolution in aqueous solution. The use of shallow V⁴⁺/V³⁺ (VO₂) and V³⁺/V²⁺ (V₂O₃) redox couple, pre-insertion of cations (e.g. Na⁺, Ca²⁺, Mg²⁺, NH₄⁺) and H₂O molecule can stabilize the performance. [7] Unfortunately, they inevitably lower Zn-ion storage capacity due to the decreased oxidation state of V, increased electrostatic interactions between negatively charged oxide layers and pre-inserted cations, and reduced host sites available for Zn-ion accommodation. [8]

Here, we report that an atomic layer deposition (ALD) derived V_2O_5 , unlike the other types of V_2O_5 (e.g. ball-milled and hydrothermal) reported in the literature, exhibits excellent capacity and cycle stability at both low and high current rates. We also discuss the V_2O_5 -dissolution mechanisms and role of electrolytes in performance stability, and present experimental evidences to support a new ionic storage mechanism accountable for the outstanding electrochemical performance of the ALD-derived V_2O_5 cathode.

Results and Discussion

Microstructure of ALD-V₂O₅

The surface view of ALD- V_2O_5 deposited on a commercial graphite paper is shown in **Figure 1a** of an SEM image. Compared with the original pure graphite paper, see **Figure S1**, there is no discernable difference other than that the coated sample appears to be smoother. The deposited V_2O_5 is first confirmed by Raman spectrum shown in **Figure S2**, where the Raman shifts match well to the vibrational modes associated with the orthorhombic V_2O_5 phase, as well as by XRD to be shown later.

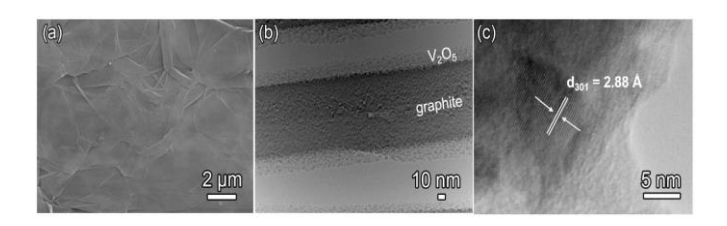


Figure 1. (a) Surface and (b) cross-sectional views of ALD- V_2O_5 overcoats on a graphite paper. (c) HRTEM image of ALD- V_2O_5 .

RESEARCH ARTICLE

The internal structure of ALD- V_2O_5 on graphite paper is revealed in **Figure 1b**, **1c** of HRTEM images, where a uniform, well-bonded, 20 nm thick V_2O_5 layer with a *d*-spacing of 2.88 Å (corresponds to the (301) planes of orthorhombic V_2O_5) is clearly seen on both sides of single graphite sheet in the graphite paper. Such a double-side coating is the result of the pre-existing gaps between each graphite sheet, thus allowing the ALD precursor and oxidizer to penetrate and react. These gaps are also expected to be filled later by the electrolyte solution during battery assembly, which are highly desirable to maximize the reactive area and ultimately boost charge transfer kinetics.

Electrochemical performance

The rate performance of ALD- V_2O_5 cathode is shown in **Figure 2a** over a current range of 2 to 20 A g^{-1} for two repeated cycles; the original discharge/charge profiles (first cycle only) are given in **Figure S3** as an example. The demonstrated reversible capacities are 496, 466, 457, 446, 430, 405 mAh g^{-1} at 2, 5, 8, 10, 15 and 20 A g^{-1} , respectively, with no sign of degradation during the two short rate excursions. Such a high-rate capability as well as current-insensitive capacity signal an excellent electrode kinetics of ALD- V_2O_5 cathode for Zn-ion storage. The Ragone plot of energy density vs power density in **Figure 2b** clearly ranks the ALD- V_2O_5 as the top performer among the pure

 V_2O_5 cathodes reported in the literature. $^{[9]}$ Obtained from CV at different scan rates (see **Figure S4**), **Figure 2c** indicates that there are only 50-70% capacitive contribution from the ALD- V_2O_5 cathode, whereas it is over 70% reported for other types of V_2O_5 cathodes in the literature. $^{[9b,\ 10]}$ The lower capacitive contribution is believed to arise from the nanoscale thickness (20 nm) of ALD- V_2O_5 , by which the diffusion of Zn-ions in the bulk becomes easier. In other words, there are ample Zn-ions penetrated the V_2O_5 bulk, rather than adsorbed on the surface.

The cycles of ALD-V $_2$ O $_5$ at both low and high rates are exceptionally stable. **Figure 2d** and **2e** show a capacity of 513 mAh g $^{-1}$ over 200 cycles and 439 mAh g $^{-1}$ over 1000 cycles at 0.5 and 5.0 A g $^{-1}$, respectively, virtually with no sign of degradation. This observation is distinctive from the literature reports that oxide-based cathodes always exhibit a poorer cycle stability at low rates than at high rates. While the nature of this phenomenon is still not well understood, most researchers attribute it to the significant surface-controlled capacitive charge storage over diffusion-controlled bulk storage. However, this understanding is contradictory to the results presented here, *viz.* a cathode with low capacitive contribution shows a good stability at low rates. Therefore, a different degradation mechanism might exist. We will discuss an alternative mechanism later.

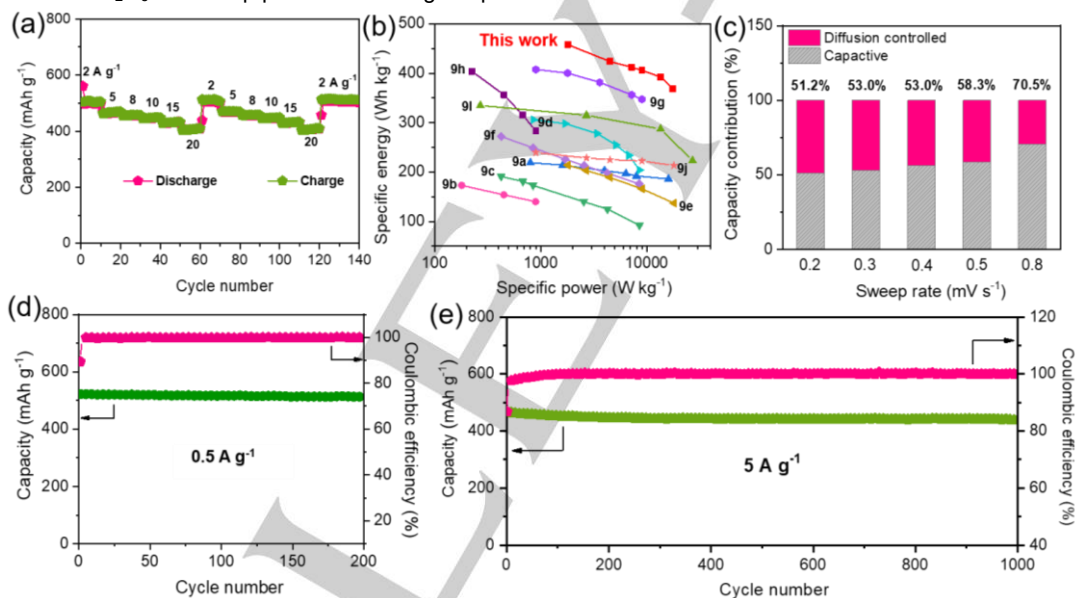


Figure 2. Electrochemical performance of ALD- V_2O_5 cathode. (a) Rate performance. (b) Ragone plot and comparison with other V_2O_5 cathodes. (c) Charge storage contribution vs voltage sweep rate in CV. (d) Cyclic performance at 0.5 A g⁻¹ and the corresponding Coulombic efficiency. (e) Cyclic performance at 5 A g⁻¹ and the corresponding Coulombic efficiency.

Morphology change vs cycling

To understand the origin of the high electrochemical performance, we first examined morphologies of the ALD- V_2O_5 cathode after testing. **Figure 3** depicts that a new flake-like phase is formed on the surface of ALD- V_2O_5 at various cycling stages. A close comparison within **Figure 3** suggests that this new phase first emerges in smaller flake-like clusters, then grows into larger flakes with cycling; the longer the cycle the more flake-like clusters formed. We also observe that such a surface morphology change is somewhat dependent of current density, i.e. at higher 5 A g⁻¹, SEM images of **Figure S5** suggests a lesser surface morphology change than at lower 0.5 A g⁻¹ for the initial cycles, but eventually a full change to the nanoflake structure after 1000 cycles.

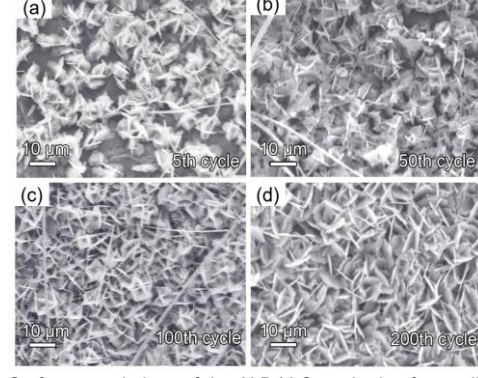


Figure 3. Surface morphology of the ALD- V_2O_5 cathode after cycling at 0.5 A g^{-1} .

In-situ and ex-situ transmissive XRD investigation

To investigate when and what the new phase is formed, we carried out ex-situ and in-situ transmissive XRD on ALD-V₂O₅ and ball-milled (BM) V₂O₅ cathodes at different state of charge (SOC), respectively. In this study, we first started with in-situ XRD on ALD-V₂O₅. Unfortunately, the signal from the ALD-V₂O₅ was too weak to discern due to the low mass loading and attenuation by the Kapton film and graphite substrate. Thus, we only performed ex-situ XRD on ALD-V₂O₅. **Figure 4a** shows that the original V₂O₅ phase appears to have changed into a different phase with a characteristic peak at ~12.3°. In the following, we will provide evidence to show that this new phase belongs to $Zn_3V_2O_7(OH)_2$ - $2H_2O$ (denoted as ZVO hereinafter). Similar to

 V_2O_5 , ZVO with space group $P\overline{3}m1$ and lattice parameters: a=2.531(5) Å and c = 6.713(5) Å also has a layered structure consisting of V-O-V pillars in V_2O_7 layers and H_2O between the layers.^[11] Early studies have suggested that it is an intercalatable material for Zn-ions (and also likely protons) with a low band gap (0.051 vs 2.163 eV for V_2O_5), ^[12, 13] Indeed, **Figure 4a** indicates lattice expansion and contraction in ZVO upon discharging and charging, respectively, as evidenced by a shift of the characteristic peak (12.3°) related to the (001) plane toward lower degree (11°) upon discharging of Zn-ion (and/or proton) intercalation. Upon charging of Zn-ion (and/or proton) deintercalation, ZVO's lattice resumes to its original state, regardless it is the 5th or 50th cycle.

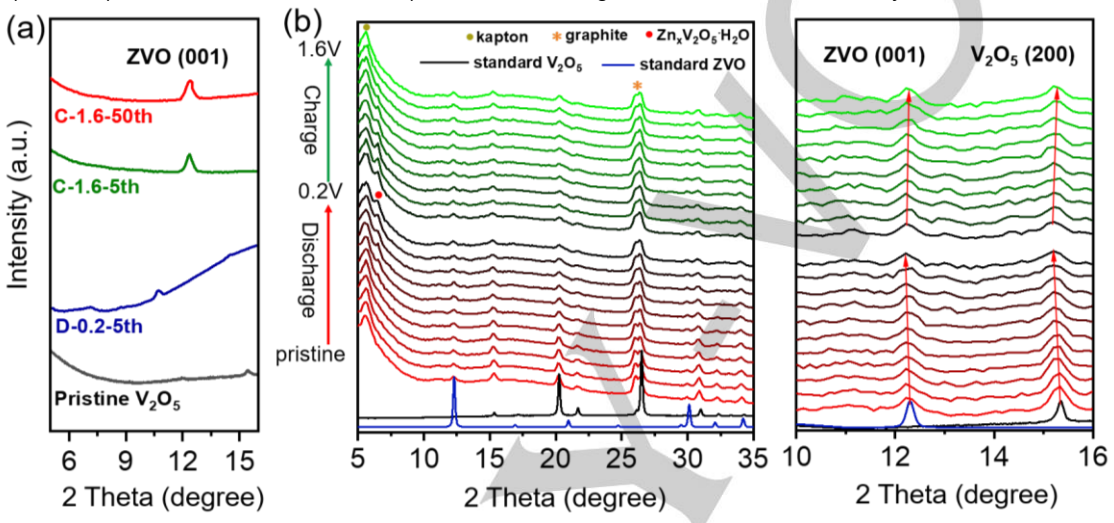


Figure 4. (a) Ex-situ XRD patterns of (001) Bragg peak of ZVO in the ALD-V₂O₅ electrode during the 5th and 50th charge and discharge states. (b) in-situ XRD patterns of BM-V₂O₅ cathode for the first cycle. Data in (b) are shifted vertically for clarity.

A supporting evidence to the ZVO formation is also provided by Figure 4b of in-situ XRD patterns collected from a BM-V₂O₅ blended with binder and conductive carbon. The corresponding charge/discharge curve is shown in Figure S6. With a much higher loading, we were able to observe the phase evolution with SOCs. The XRD patterns include the characteristic peaks of orthorhombic V₂O₅ (15.3°, 20.3°, 22°, 31°) and graphite (26°) in the initial state. Upon discharging, the peak at 15.3° (see the right panel) slightly shifts toward lower degree and a new peak emerges at 6.24° (see red dot in the left panel); the latter can be assigned to layered $Zn_xV_2O_5{\cdot}nH_2O$ due to the co-insertion of Zn2+ and H2O,[9g, 14] which it is not observable for the ALD-V2O5 sample. Nonetheless, the cycle for the BM-V₂O₅ does not seem to be fully reversible as the V₂O₅ peaks (15.3°) becomes weaker with cycling, signaling that V_2O_5 is being consumed. One possibility is that it irreversibly converts into ZVO; the latter is suggested by the right panel of Figure 4b by the emergence of 12.3°-peak and its small left-shift during the discharging cycle and its persistence, and slight right-shift during the charging cycle, even though its overall intensity is rather weak. The weak ZVO signal is due to the slow V₂O₅-to-ZVO conversion kinetics in $BM-V_2O_5$ compared to $ALD-V_2O_5$. We will present more

evidence to this assertion in a later section. Overall, the trending of these ZVO peak shifts corresponds well to **Figure 4a**.

Ex-situ microscopic and surface chemistry analyses

STEM mapping, HRTEM and XPS of the ALD-V₂O₅ cathode were also employed to gather information on chemical compositions and oxidation states in V₂O₅ vs SOCs. Figure 5a of STEM elemental mapping shows expectedly no Zn but V in the pristine ALD-V₂O₅. Upon a full discharge to 0.2 V at the 20th cycle, for example, a significant amount of Zn is observed along with V in the sample, implying incorporation of Zn, while the morphology is also transformed into the "flake-like" shape, matching well to those observed in Figure 3. Upon a full charge to 1.6 V at the 20th cycle, both V and Zn are detectable, but with a reduced amount of Zn. This "permanent" Zn in the sample is persistent even after 50 cycles. The corresponding STEM-EDS results in Figure S7 complements the STEM-mapping, revealing an atomic V/Zn ratio of 0.45 after a full discharge to 0.2 V at the 20th cycle, and V/Zn= 0.61 upon a full charge to 1.6 V; the latter remains almost unchanged (V/Zn=0.62) after a full charge to 1.6 V at the 50 cycle, which is very close to the stoichiometric ratio of V/Zn=0.67 in ZVO, indicating possible formation of ZVO and its stability during cycling.

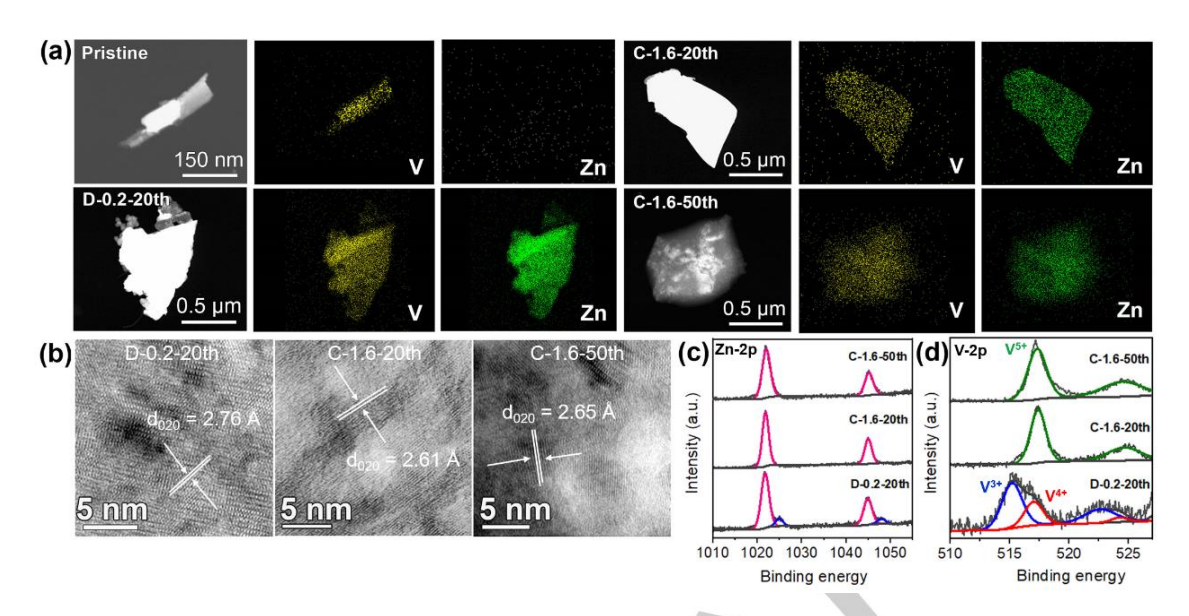


Figure 5. Compositional analysis of ALD- V_2O_5 cathode at different charge and discharge states. (a) STEM images with Zn and V mapping at states of pristine and discharged to 0.2 V after 20 cycles (D-0.2-20th), charged to 1.6 V after 20 cycles (C-1.6-20th), and charged to 1.6 V after 50 cycles (C-1.6-50th). HRTEM images of ALD- V_2O_5 at (b) D-0.2-20th, C-1.6-20th, and C-1.6-50th states, respectively. (c) Zn-2p and (d) V-2p XPS spectra of the samples at D-0.2-20th, C-1.6-20th, and C-1.6-50th states, respectively.

Figure 5b of HRTEM images further suggests that the incorporation and removal of Zn-ion (and/or proton) into and from the sample are accompanied by a change in the (020) interlayer d-spacing of ZVO, i.e. from 2.61 Å of the pristine ZVO to 2.76 Å after a full discharge and back to 2.62 and 2.65 Å after a full charge at the 20th and 50th cycles, respectively. Figure 5c and 5d of subsequent XPS analysis indicates the presence of Zn²⁺ (Zn-2p 3/2 at 1021.6 eV and Zn-2p 1/2 at 1045.1 eV) and V5+ (V-2p 3/2 at 517.4 eV and V-2p 1/2 at 524.80 eV) for all charged states. Meanwhile, a second low-intensity Zn²⁺ peak (Zn-2p 3/2 at 1025 eV and Zn-2p 1/2 at 1048 eV, marked as the blue curve in **Figure 5c**) and V⁴⁺/V³⁺ redox couples (V⁴⁺ at 517 eV and V3+ at 515 eV) are observed at the discharged state, signifying the intercalation of Zn2+ and the associated oxidationstate change in V-lattice. [9d, 15] Overall, the results of STEM mapping, STEM-EDS, HRTEM and XPS suggest that there might be a new Zn-ion storage mechanism in the ALD-V₂O₅ involving ZVO as the Zn-ion storage material, not in the V2O5 as originally thought.

Understanding the dissolution of V₂O₅ in aqueous solutions

It is well known that crystalline V_2O_5 is slightly soluble in water, giving a characteristic pale-yellow color. According to the pH-log[V⁵⁺] diagram, see **Figure 6**,[¹6] at pH < 3.2 and [V⁵⁺] < 10⁻¹ M (pH dependent), the most stable form of V-species in an aqueous solution is VO_2^+ :

$$V_2O_5 + 2H^+ = 2VO_2^+ + H_2O$$
 (1)

leading to an increase in pH by consuming protons. However, at $3.8 \le \text{pH} \le 7.8$ and [V⁵⁺] < $10^{-4}\,\text{M}$, the most stable V-species is $VO_2(OH)_2$ - (or H_2VO_4 -) and the V_2O_5 dissolution follows:

$$V_2O_5 + 3H_2O = 2VO_2(OH)_2^- + 2H^+$$
 (2)

resulting in a decrease in pH by releasing protons. The formed $VO_2(OH)_2$ can further react with Zn^{2+} in Zn-salt, yielding ZVO via the following reaction:

 $2VO_2(OH)_2$ + $3Zn^{2+} + 3H_2O = Zn_3V_2O_7(OH)_2 \cdot 2H_2O$ (ZVO) + $4H^+$ (3) Our independent $V_2O_5/electrolyte$ reaction experiments agree well with the pH-log [V $^{5+}$] diagram. **Figure S8** explicitly shows that the initial pH values of 3M Zn(NO $_3)_2$ and 3M ZnSO $_4$ electrolytes have been increased, *i.e.* $3.14 \rightarrow 3.58$ for ZnSO₄ and $3.06 \rightarrow 3.52$ for Zn(NO₃)₂ after soaking with V₂O₅. In this case (initial pH < 3.2), the stable V-species in the solution is VO₂⁺ accompanied by consuming protons. **Figure S9** of XRD confirms that there is no new phase formation in the original V₂O₅. For 3M ZnCl₂ with a starting pH = 3.8, which is on the boundary of VO(OH)₃ and VO₂(OH)₂⁻, only a very small pH change, *i.e.* $3.8 \rightarrow 3.77$, was observed. The XRD pattern correspondingly indicates a minor fraction of ZVO.

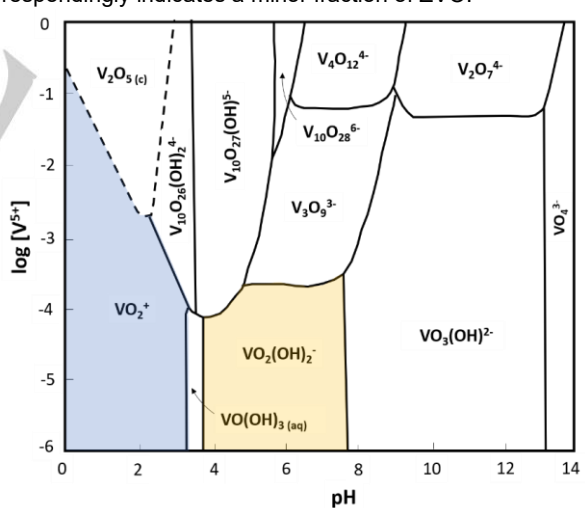


Figure 6. The pH-log [V⁵⁺] diagram in V₂O₅-H₂O system.

For the 3M Zn(CF₃SO₃)₂ electrolyte with a starting pH = 3.95, **Figure 7a** shows that its pH rapidly decreases during the first 5-days of soaking, followed by leveling off at pH ~2.5. This pH decrease can be explained by reaction (2) with VO₂(OH)₂⁻ being the stable V-species and release of protons. The VO₂(OH)₂⁻ species can further react with Zn²⁺ to form ZVO as shown by reaction (3). Indeed, **Figure 7b** of XRD patterns indicates that the original V₂O₅ structure has been completely transformed into ZVO. The Rietveld refinement in **Figure 7c** using ZVO as the model indicates low reliability factors of R_{wp} = 3.29 % and R_p = 2.92 %. **Figure 7d** and **7e** of XPS analysis complements the

XRD data by showing that Zn^{2+} and V^{5+} are the only two cations in the sample after soaking in the electrolyte, but not in that soaked in a pure H_2O . Another contributing factor to the ZVO formation could be attributed to the bulky $CF_3SO_3^-$ anion. While the doubly charged Zn^{2+} is favorable to a stronger solvation, the

presence of bulky singly charged $CF_3SO_3^-$ can effectively shield H_2O molecules from coordinating with Zn^{2+} , thus reducing the solvation effect and giving Zn^{2+} more freedoms to move and react with $VO_2(OH)_2^{-}$.[2a, 17]

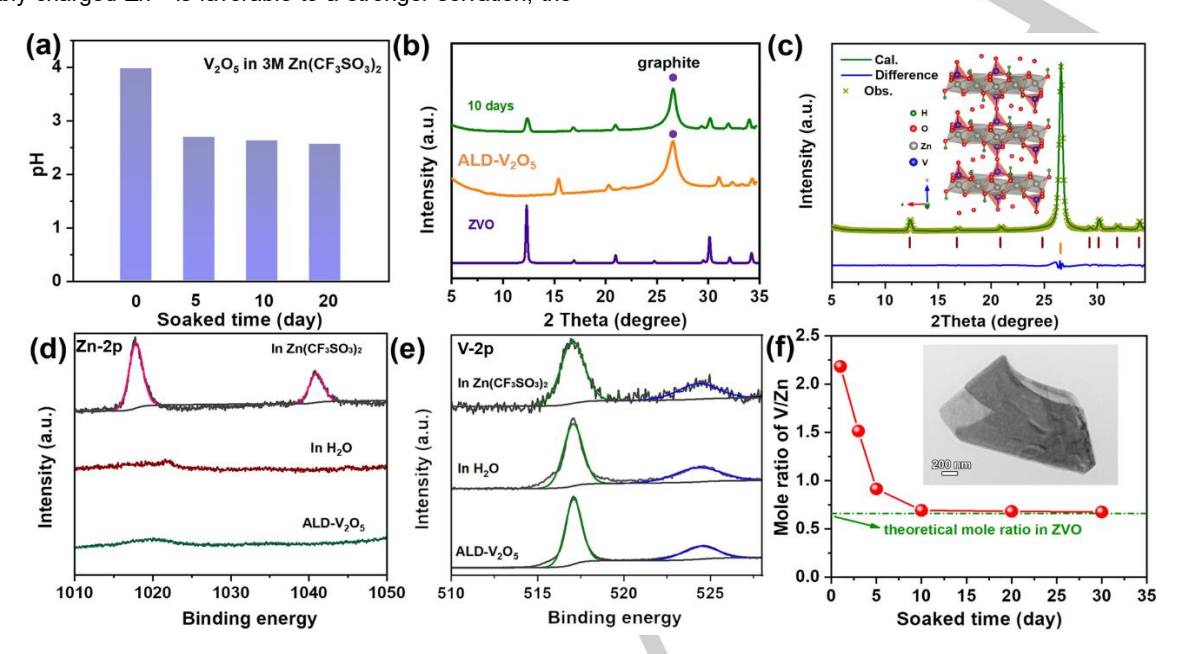


Figure 7. (a) pH values vs the soaking time of ALD- V_2O_5 in 3M Zn(CF₃SO₃)₂. (b) XRD patterns ALD- V_2O_5 at pristine and after soaking in 3M Zn(CF₃SO₃)₂ electrolyte for 10 days. (green: soaked V_2O_5 , orange: pristine V_2O_5 , purple: standard ZVO). (c) Experimental and Rietveld-refined XRD patterns of the soaked ALD- V_2O_5 . Inset: crystal structures of ZVO. (d) Zn-2p and (e) V-2p XPS spectra of the pristine, soaked in H_2O_5 , and soaked in 3M Zn(CF₃SO₃)₂ samples, respectively. (f) V/Zn molar ratio in ALD- V_2O_5 vs the soaked time. The inset shows TEM image of a 10-day soaked ALD- V_2O_5 .

Additional supporting evidence to the ZVO formation is the time-dependent change in V/Zn molar ratio determined by ICP-OES. Figure 7f shows a rapid decrease in V/Zn molar ratio from ~2.25 at the beginning to 0.693 after 5 days, followed by a stabilization at 0.676 on the following 25 days; the stabilized V/Zn ratio matches well to the theoretical value of 0.67 for a pure ZVO, implying a full transformation of V₂O₅ to ZVO. The TEM image of an isolated ZVO particle shown in the inset of Figure 7f depicts a nanoflake morphology, matching to those observed in Figure 3. Since the V₂O₅-to-ZVO conversion is expected to be diffusion limited, a thicker ALD-V2O5 would take longer time to achieve a full conversion. Figure S10 compares the coverage of flake-like clusters for 20 nm and 80 nm thick ALD-V₂O₅ layers for different soaking times. The comparison suggests that thicker V₂O₅ can spontaneously transform into ZVO but may need more time to complete a full conversion, which leads to an inferior capacity retention due to the limitation in diffusion and higher resistance (Figure S11).

From the above proposed mechanism, it is important to point out that electrical cycling can accelerate the formation of ZVO. This is because H $^+$ like Zn $^{2+}$ can also be intercalated into ZVO's layered structure during a discharge process, thus shifting the reaction (3) to promote the formation of ZVO. During the charge process, the intercalated H $^+$ will move back to the electrolyte and re-establish the equilibrium of the reaction (3). Such an equilibrium-and-shift dynamics will continue until all V₂O₅ is converted into ZVO. Therefore, it is reasonable to assert that the actual transformation of V₂O₅ into ZVO in a real battery cell is faster than what **Figure 7f** indicates. The feasibility of H $^+$ intercalation is confirmed by the fact that ALD-V₂O₅ cathode

exhibits lower capacity and higher overpotential in organic-based electrolytes than in aqueous electrolytes, see **Figure S12**. Another supporting evidence is the ionic diffusivity obtained from GITT technique (**Figure S13**). The extracted ionic diffusivity shown in **Figure S14** is comparable to those of other reported vanidium oxide cathodes. [9g, 13b] More importantly, it indicates a higher value at high voltage region than at low voltage region, implying H $^+$ involvement in diffusion at high voltage given the high-mobility nature of H $^+$. This observation is consistent with early theoretical and experimental results regarding the likelihood of Zn $^{2+}$ /H $^+$ co-intercalation. [7b, 18]

Based on above results, the electrochemical mechanism of Zn/ALD-V $_2$ O $_5$ batteries with 3M Zn(CF $_3$ SO $_3$) $_2$ electrolyte can be described by two stages: (1) the pristine ALD-V $_2$ O $_5$ initially involves in ionic intercalation/extraction and transformation into ZVO. The formed ZVO can also be a host for co-Zn $^{2+}$ /H $^+$ intercalation/extraction; (2) after V $_2$ O $_5$ is completely converted into ZVO, the latter acts as the only host for Zn $^{2+}$ /H $^+$ -storage.

Note that a potential consequence of the reaction (3) is the partial consumption of Zn^{2+} and H_2O in the electrolyte, which may change the electrical property of the electrolyte solution. As such, the initial relative mass of electrolyte to V_2O_5 should be ensured high enough to support the transformation while maintaining the basic properties of the electrolyte.

Further electrochemical testing

Following the above discussion, a legitimate question to ask is if the *in-situ* formation of ZVO in ALD- $V_2O_5/3M$ Zn(CF₃SO₃)₂ cell is indeed the reason for the observed extraordinary capacity and stability. To answer this question, we tested three additional cells: a Zn(CF₃SO₃)₂-presoaked ALD- $V_2O_5/3M$ Zn(CF₃SO₃)₂ cell,

a premade ZVO/3M Zn(CF₃SO₃)₂ cell and ALD-V₂O₅/3M ZnSO₄ cell. Note the premade ZVO was synthesized by following a previously reported hydrothermal method [5, 6] and made into a testable electrode by mixing it with binder, conductive carbon, and solvent; its phase verification/morphology can be found in Figure S15. Figure 8a of capacity retention comparison shows that the pre-soaked ALD-V₂O₅ performs slightly better than the pristine one, which is likely caused by a minor change in the electrolyte properties due to the in-situ transformation. However, with the same 3M Zn(CF₃SO₃)₂ as the electrolyte, both ALD-V₂O₅ cathodes outperform substantially the prefabricated ZVO in cycle stability. We attribute such an excellent stability to the unique properties possessed by the ALD-V₂O₅ derived cathode: nanosized ZVO flakes well bonded to a conductive graphite substrate, high reactive surface area, nanoscale thickness and binder-free composition, all of which would facilitate Zn-ion transport and promote the best utilization of the active material. On the other hand, the ALD-V₂O₅/ZnSO₄ cell also exhibits a worse capacity retention than the ALD-V₂O₅/3M Zn(CF₃SO₃)₂ cells. We attribute it to the V₂O₅ dissolution in ZnSO₄ electrolyte via reaction (1), thus a gradual loss of the active V₂O₅. Figure **8b** compares the differential capacitance plots (dQ/dV vs V) for the pristine, presoaked $ALD-V_2O_5$ and pure ZVO. A general trend is that all the redox peaks of ALD-V₂O₅ related samples shift toward those of ZVO with cycling, suggesting a transition from V_2O_5 to ZVO.

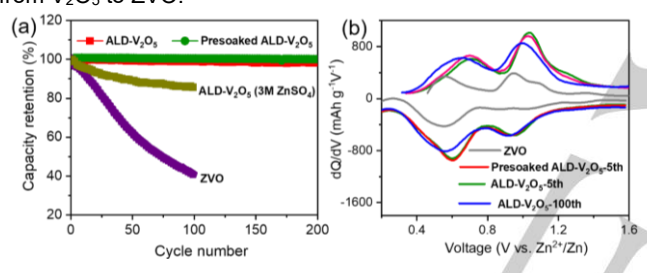


Figure 8. (a) Cyclic stability comparison among the pristine ALD-V₂O₅, presoaked ALD-V₂O₅, ZVO cathodes in 3M Zn (CF₃SO₃)₂ electrolyte and pristine ALD-V₂O₅ in 3M ZnSO₄ at 0.5 A g⁻¹. (b) The dQ/dV comparison at the selected cycles.

In addition, the corrosion of Zn-anode can also contribute to the degradation. It has been previously reported that Zn-anode is thermodynamically and electrochemically unstable in aqueous electrolytes.^[19] The SEM images of **Figure S16** for Zn-anode after cycles indeed show a gradual increase in surface roughness. Such a roughened morphology would accelerate the uneven nucleation, promoting Zn dendrite formation and resulting in capacity deterioration. Further work is needed to address this issue.

Finally, the conversion kinetics from V_2O_5 to ZVO was studied among different types of V_2O_5 in particle sizes of 1-5 µm and 0.1-0.2 µm, which were fabricated by ball-milling (named as BM- V_2O_5) and hydrothermal (named as HT- V_2O_5) methods, respectively. Detailed fabrication procedures and the particle morphology are provided in the Supporting Information (SI) and **Figure S17**, respectively. Due to the largest sizes and lowest surface areas, both the soaking experiment and electrochemical measurements confirm that BM- V_2O_5 takes the longest time to convert to ZVO (see **Figure S18-26**), thus having the worst cycle stability. Another factor to the inferior performance of both BM- V_2O_5 and HT- V_2O_5 is the use of binder and conductive carbon in its electrode makeup, which could interrupt electron

pathways by the ZVO transformation and phase reconstruction. To support this point, a conventional flake-like V_2O_5 was also synthesized and then fabricated into a traditional slurry-coated cathode. The performance in **Figure S27** clearly shows a faster capacity decay than the above ALD- V_2O_5 based cathode. Finally, we emphasize that the capacity reported in this study is based on the mass of V_2O_5 . We did not use ZVO mass to present the capacity because the ZVO mass is varying throughout the cycle. However, if we assume all the V_2O_5 is converted into ZVO, the capacity would be very close to the reported ZVO's capacities (~ 198 mAh g-1). [13]

Conclusion

In summary, we have demonstrated that ALD-V₂O₅ is a high capacity and durable cathode with Zn(CF₃SO₃)₂ electrolyte for ZIBs. We observe that V₂O₅ atomic layers transform into ZVO nanoflakes in-situ in a 3M Zn(CF₃SO₃)₂ electrolyte and ZVO becomes the active materials for the subsequent Zn²⁺/H⁺ storage. A determining factor for the ZVO formation is the initial pH of the electrolyte, i.e. the most stable V-species is VO₂⁺ at pH < 3.2 and it is $VO_2(OH)_2$ at 3.8 \leq pH \leq 7.8. Therefore, for 3M $ZnSO_4$ and $3M Zn(NO_3)_2$ electrolytes with a pH < 3.2, there is no new phase formation, but partial dissolution; whereas for 3M $Zn(CF_3SO_3)_2$ and 3M $ZnCl_2$ electrolytes with a pH \geq 3.8, ZVO phase is formed as a result of VO₂(OH)₂- reaction with Zn²⁺. Since ZVO is also a good Zn²⁺/H⁺ host, the sustainable capacity observed in ALD-V₂O₅/3M Zn(CF₃SO₃)₂ cell is derived from Zn²⁺/H⁺ (de)intercalation in ZVO. Due to the H⁺ co-intercalation, electrical cycling can accelerate the V₂O₅-to-ZVO conversion. Benefited from the strong bonding, high-surface-area, nanosized thickness and absence of binder, the in-situ converted ZVO cathode outperforms substantially the ball-milled hydrothermal V₂O₅, exhibiting a facile electrokinetics that results in a high capacity of 513 mAh g⁻¹ at 0.5 A g⁻¹ for 200 cycles and 439 mAh g-1 at 5 A g-1 for 1000 cycles without detectable degradation. Our demonstration of ALD-V₂O₅ as a high-capacity and durable cathode and the gained fundamental insights into the in-situ conversion and V2O5-dissolution mechanisms are expected to help advance the cathode development for commercial ZIBs.

Acknowledgements

KH acknowledges the financial support from the South Carolina SmartState program and National Science Foundation under award number DMR-1464112 and CBET-1801284. W.V.D.B. and M.S. acknowledge support by the National Science Foundation (DMR-1752615). This work made use of the South Carolina SAXS Collaborative.

Keywords: capacity • stability • V_2O_5 dissolution • electrolyte • cathode

a) F. Wan, Z. Niu, Angew. Chem. Int. Ed. 2019, 58, 16358; b) L. Chen, Q.
 An, L. Mai, Adv. Mater. Interfaces 2019, 6, 1900387; c) H. Li, L. Ma, C.
 Han, Z. Wang, Z. Liu, Z. Tang, C. Zhi, Nano Energy 2019, 62, 550.

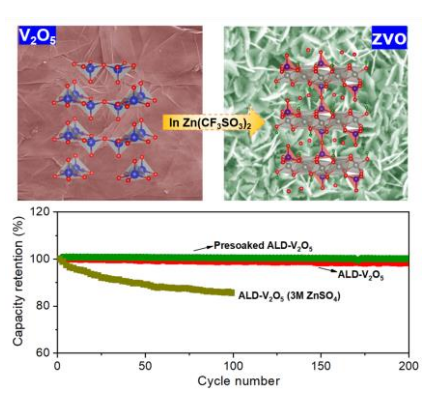
- [2] a) S. Huang, J. Zhu, J. Tian, Z. Niu, Chem.: Eur. J. 2019, 25, 14480; b) M. Song, H. Tan, D. Chao, H. J. Fan, Adv. Funct. Mater. 2018, 28, 1802564;
 c) Q. Yang, G. Liang, Y. Guo, Z. Liu, B. Yan, D. Wang, Z. Huang, X. Li, J. Fan, C. Zhi, Adv. Mater. 2019, 31, 1903778.
- [3] a) D. Selvakumaran, A. Pan, S. Liang, G. Cao, J. Mater. Chem. A 2019, 7, 18209; b) L. Chen, Q. An, L. Mai, Adv. Mater. Interfaces 2019, 6, 1900387. c) P. Hu, Z. Zou, X. Sun, D. Wang, J. Ma, Q. Kong, D. Xiao, L. Gu, X. Zhou, J. Zhao, S. Dong, B. He, M. Avdeev, S. Shi, G. Cui, L. Chen, Adv. Mater. 2020, 32, 1907526.
- [4] a) B. Tang, L. Shan, S. Liang, J. Zhou, Energy Environ. Sci. 2019, 12, 3288; b) X. Gao, H. Wu, W. Li, Y. Tian, Y. Zhang, H. Wu, L. Yang, G. Zou, H. Hou, X. Ji, Small 2020, 1905842.
- [5] a) M. H. Alfaruqi, V. Mathew, J. Gim, S. Kim, J. Song, J. P. Baboo, S. H. Choi, J. Kim, *Chem. Mater.* 2015, 27, 3609; b) Y. Lu, Y. Wen, F. Huang, T. Zhu, S. Sun, B. C. Benicewicz, K. Huang, *Energy Storage Mater.* 2020, 27, 418
- [6] a) J. Yao, Y. Li, R. C. Massé, E. Uchaker, G. Cao, Energy Storage Mater. 2018, 11, 205; b) N. Zhang, F. Cheng, J. Liu, L. Wang, X. Long, X. Liu, F. Li, J. Chen, Nat. Commun. 2017, 8, 1; c) X. Liu, J. Yi, K. Wu, Y. Jiang, Y. Liu, B. Zhao, W. Li, J. Zhang, Nanotechnology 2020, 31, 122001.
- [7] a) L. Wang, K. Huang, J. Chen, J. Zheng, Sci. Adv. 2019, 5, eaax4279; b) F. Ming, H. Liang, Y. Lei, S. Kandambeth, M. Eddaoudi, H. N. Alshareef, ACS Energy Lett. 2018, 3, 2602; c) S. Gu, H. Wang, C. Wu, Y. Bai, H. Li, F. Wu, Energy Storage Mater. 2017, 6, 9.
- [8] a) Y. Yang, Y. Tang, G. Fang, L. Shan, J. Guo, W. Zhang, C. Wang, L. Wang, J. Zhou, S. Liang, *Energy Environ. Sci.* 2018, 11, 3157; b) P. He, G. Zhang, X. Liao, M. Yan, X. Xu, Q. An, J. Liu, L. Mai, *Adv. Energy Mater.* 2018, 8, 1702463.
- [9] a) P. Hu, M. Yan, T. Zhu, X. Wang, X. Wei, J. Li, L. Zhou, Z. Li, L. Chen, L. Mai, ACS Appl. Mater. Interfaces 2017, 9, 42717; b) D. Xu, H. Wang, F. Li, Z. Guan, R. Wang, B. He, Y. Gong, X. Hu, Adv. Mater. Interfaces 2019, 6, 1801506; c) H. Qin, L. Chen, L. Wang, X. Chen, Z. Yang, Electrochimica Acta 2019, 306, 307; d) Y. Li, Z. Huang, P. K. Kalambate, Y. Zhong, Z. Huang, M. Xie, Y. Shen, Y. Huang, *Nano Energy* **2019**, 60, 752; e) Y. Lu, T. Zhu, N. Xu, K. Huang, ACS Appl. Energy Mater. 2019, 2, 6904; f) D. Chen, X. Rui, Q. Zhang, H. Geng, L. Gan, W. Zhang, C. Li, S. Huang, Y. Yu, Nano Energy 2019, 60, 171; g) N. Zhang, Y. Dong, M. Jia, X. Bian, Y. Wang, M. Qiu, J. Xu, Y. Liu, L. Jiao, F. Cheng, ACS Energy Lett. 2018, 3, 1366; h) M. S. Javed, H. Lei, Z. Wang, B. Liu, X. Cai, W. Mai, Nano Energy 2020, 70, 104573; I) M. Yan, P. He, Y. Chen, S. Wang, Q. Wei, K. Zhao, X. Xu, Q. An, Y. Shuang, Y. Shao, K. T. Mueller, L. Mai, J. Liu, J. Yang, Adv. Mater. 2018, 30, 1703725; j) X. Wang, Y. Li, S. Wang, F. Zhou, P. Das, C. Sun, S. Zheng, Z. S. Wu, Adv. Energy Mater. 2020, 2000081.
- [10] a) B. He, Z. Zhou, P. Man, Q. Zhang, C. Li, L. Xie, X. Wang, Q. Li, Y. Yao, J. Mater. Chem. A 2019, 7, 12979; b) X. Wang, L. Ma, J. Sun, ACS Appl. Mater. Interfaces 2019, 11, 41297.
- [11]P. Y. Z. Thomas Chirayil, M. Stanley Whittingham, *Chem. Mater.* 1998, 10, 2629
- [12] A. Jain, S.P. Ong, G. Hautier, W. Chen, W.D. Richards, S. Dacek, S. Cholia, D. Gunter, D. Skinner, G. Ceder, K.A. Persson, APL Mater. 2013, 1, 011002.
- [13] a) Z. Pan, J. Yang, J. Yang, Q. Zhang, H. Zhang, X. Li, Z. Kou, Y. Zhang, H. Chen, C. Yan, J. Wang, ACS Nano 2020, 14, 842; b) C. Xia, J. Guo, Y. Lei, H. Liang, C. Zhao, H. N. Alshareef, Adv. Mater. 2018, 30, 1705580.
- [14] D. Kundu, B. D. Adams, V. Duffort, S. H. Vajargah, L. F. Nazar, *Nat. Energy* 2016, 1, 16119.
- [15] J. Zhou, L. Shan, Z. Wu, X. Guo, G. Fang, S. Liang, Chem. Commun. 2018, 54, 4457.
- [16] C. Baes, R. Mesmer, Wiley-Interscience, New York 1976, 177.
- [17] N. Zhang, F. Cheng, Y. Liu, Q. Zhao, K. Lei, C. Chen, X. Liu, J. Chen, J. Am. Chem. Soc. 2016, 138, 12894.
- [18] a) S. Liu, L. Kang, J. M. Kim, Y. T. Chun, J. Zhang, S. C. Jun, Adv. Energy Mater. 2020, 2000477; b) R. Li, H. Zhang, Q. Zheng, X. Li, J. Mater. Chem. A 2020, 8, 5186; c) F. Wan, L. Zhang, X. Dai, X. Wang, Z. Niu, J. Chen, Nat. Commun. 2018, 9, 1656; d) K. Zhu, T. Wu, S. Sun, W. Bergh, M. Stefik, K. Huang, Energy Storage Mater. 2020, 29, 60; e) W. Liu, L. Dong, B. Jiang, Y. Huang, X. Wang, C. Xu, Z. Kang, J. Mou, F. Kang, Electrochim. Acta 2019, 320, 134565; f) Q. Zhao, L. Liu, J. Yin, J.

- Zheng, D. Zhang, J. Chen, L. A. Archer, *Angew Chem. Int, Ed.* **2020**, 59, 3048.
- [19] a) Z. M. Zhao, J. W. Zhao, Z. L. Hu, J. D. Li, J. J. Li, Y. J. Zhang, C. Wang, G. L. Cui, *Energy Environ. Sci.* 2019, 12, 1938; b) J. W. Zhao, J. Zhang, W. H. Yang, B. B. Chen, Z. M. Zhao, H. Y. Qiu, S. M. Dong, X. H. Zhou, G. C. Lei, L. Q. Chen, *Nano Energy* 2019, 57, 625.



1

Entry for the Table of Contents



4

We report on the of atomic layer deposition derived V_2O_5 (ALD- V_2O_5) as a high-capacity and stable ZIB cathode. Direct and compelling evidences show that ALD- V_2O_5 undergoes an *in situ* on-site transformation into nanoscaled $Zn_3V_2O_7(OH)_2\cdot 2H_2O$ (ZVO) and the latter is largely responsible for the excellent electrochemical performance. We also offer our new understanding on the capacity degradation mechanisms.

